Effect of Ba Content on Oxygen Permeation Performance of $Ba_xSr_{1-x}Co_{0.8}Fe_{0.2}O_{3-\delta}$ ($x = 0.2$, 0.5, and 0.8) Perovskite-Type Membrane

Mohammad Ali Alaee, Mohammad Mehdi Movahednia, and Toraj Mohammadi*

Research Centre for Membrane Separation Processes, Faculty of Chemical Engineering, Iran University of Science and Technology, Narmak, Tehran, Iran

A perovskite-type $Ba_{(x=0.2,0.5,0.8)}Sr_{1-x}Co_{0.8}Fe_{0.2}O_{3-\delta}$ (BSCFO) was synthesized and used as an oxygen permeable membrane. The oxygen permeation flux of the membranes with a thickness of 4 mm was determined at different temperatures, feed flow rates (air), and helium flow rates between (650 and 950) °C, (100 and 200) mL·min^{-1}, and (40 and 80) mL·min^{-1}, respectively. Experimental results showed that increasing helium flow rate increases oxygen permeation flux due to reduction of oxygen partial pressure in the permeate side. However, it was realized that oxygen permeation flux could be affected by air flow rate in the feed side. The dependency of oxygen permeation flux on air flow rate decreases at air flow rates higher than 150 mL·min^{-1}. Although XRD and EDS results showed that the surface of the BSCFO membranes exposed to air for 75 h is almost similar to the surface of the fresh membranes in composition and structure, there are differences between the fresh membrane surface and the membrane surface exposed to helium, due to the reduction reaction. Comparing SEM images of the used membrane surfaces exposed to air and helium showed that the Ba content of $Ba_{0.8}Sr_{0.2}Co_{0.8}Fe_{0.2}O_{3-\delta}$ makes the most oxygen permeation, while the Ba content of $Ba_{0.2}Sr_{0.8}Co_{0.8}Fe_{0.2}O_{3-\delta}$ makes the highest stability.

1. Introduction

During recent years, because of a huge amount of existing and discovered natural gas resources which have never been fully developed due to their remoteness, small extensive efforts have been made on both direct and indirect conversions of methane. The direct conversion involves oxidative coupling of methane to ethylene and selective oxidation of methane to methanol and formaldehyde. The indirect conversion involves reforming of natural gas to syngas ($CO + H_2$) and then using syngas to produce a series of important chemical products such as liquid fuels and methanol.[1]

The manner in which syngas is produced can be influenced by the need for oxygen enrichment facilities.[2] Membrane reactors have attracted increasing attention for syngas production because they have advantages of simple design and saving energy.[3] By providing oxygen at low costs, the membrane processes can lower the cost of the syngas production process.[2]

Dense ceramic membranes exhibiting mixed oxygen ionic and electronic conductivity (MIECM) provide a new way for oxygen production. At high temperatures with the presence of an oxygen partial pressure gradient across the membrane, oxygen can permeate through the MIECM with infinite permselectivity.[4,5] Compared with industrial scale methods of pressure swing adsorption and cryogenic separation, these ceramic membranes have an advantage of continuous oxygen production. MIECMs also found promising applications in partial oxidation of light hydrocarbons,[6−9] waste reduction, and recovery, etc.[10,11]

A vast range of mixed conducting materials are perovskites, with a basic orthorhombic structure, that makes these materials very stable at high temperatures. An excellent review about the perovskite family structure has been carried out by Roy.[12,13]

The general formula for these materials can be represented as ABO_3, or for doped perovskites as $A_{1-x}A'_xB_{1-y}B'_yO_{1-\delta}$, where x and y are fractions of dopants in A and B sites, respectively, and δ is the number of oxygen vacancies.

Doping of oxygen-conducting ceramics with multivalent cations can lead to simultaneous occurrence of ionic and electronic conductivity. Oxygen transport through such membranes can occur only via hopping oxygen ions to neighboring vacant sites in the crystal lattice of mixed conductors.[14]

In the ideal perovskite structure ABO_3, the sum of A-site and B-site cation valences is +6, and therefore no oxygen vacancy exists. However, in $A_xA'_{1-x}B_{1-y}B'_yO_{3-\delta}$, perovskite oxygen vacancy appears to compensate for the difference in the valence of cation and oxygen ions. So, oxygen vacancy is responsible for electrical neutrality, and wherever electrical neutrality is disrupted, the formation of vacancy balances it.[15]

As has been known, the perovskite structure is preserved if the tolerance factor is between 0.8 and 1. The tolerance factor of $Ba_xSr_{1-x}Co_{0.8}Fe_{0.2}O_{3-\delta}$ increases with increasing Ba because the ionic radius of Ba is larger than Sr. Increasing the tolerance factor is responsible for instability of the membrane with a higher doping level of Ba.[16]

At high temperatures, with the presence of an oxygen partial pressure gradient across the membrane, oxygen molecules on the high oxygen pressure side are adsorbed on the membrane surface and dissociated into oxygen ions, which then migrate through the bulk via the oxygen vacancies to the membrane surface of the opposite side, where the oxygen ions are recombined with electron holes to form oxygen molecules. Electrons migrate through the membrane in a direction opposite to the oxygen ions to keep local electrical neutrality, whereas the transport of any other species is excluded. This electron

* Corresponding author. Tel.: +98(21)77240496. Fax: +98(21)77240495. E-mail: torajmohammadi@iust.ac.ir.

10.1021/je9001762 CCC: $40.75
Published on Web 09/16/2009

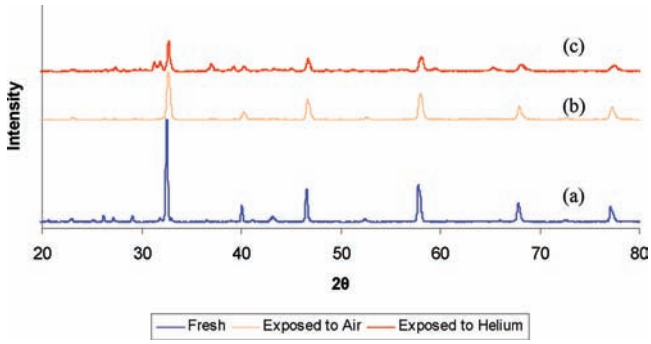

Figure 1. XRD patterns of the $Ba_{0.2}Sr_{0.8}Co_{0.8}Fe_{0.2}O_{3-\delta}$ disk membranes. (a) The fresh membrane; (b) surface of the used membrane exposed to air after 75 h oxygen permeation; (c) surface of the used membrane exposed to helium after 75 h oxygen permeation.

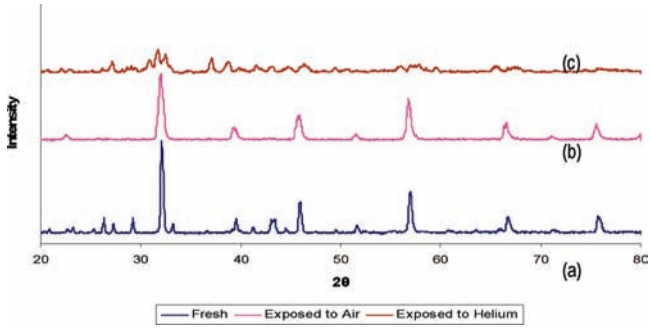

Figure 2. XRD patterns of the $Ba_{0.0.5}Sr_{0.5}Co_{0.8}Fe_{0.2}O_{3-\delta}$ disk membranes. (a) The fresh membrane; (b) surface of the used membrane exposed to air after 75 h oxygen permeation; (c) surface of the used membrane exposed to helium after 75 h oxygen permeation.

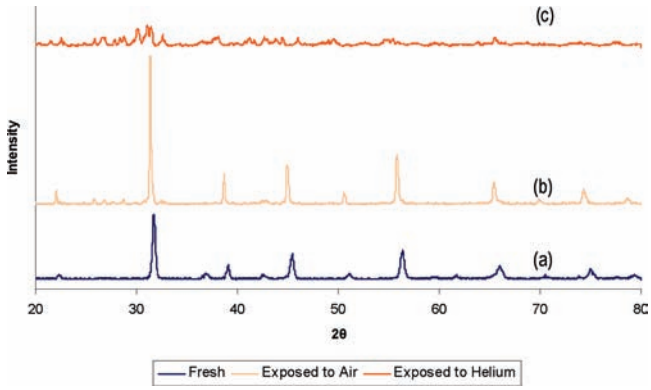

Figure 3. XRD patterns of the $Ba_{0.0.8}Sr_{0.2}Co_{0.8}Fe_{0.2}O_{3-\delta}$ disk membranes. (a) The fresh membrane; (b) surface of the used membrane exposed to air after 75 h oxygen permeation; (c) surface of the used membrane exposed to helium after 75 h oxygen permeation.

conduction proceeds via B lattice cations through strongly overlapping B−O−B bonds by a mechanism named as the Zerner double exchange process as shown below

$$B^{n+} - O^{2-} - B^{(n+1)+} \Rightarrow B^{(n+1)+} - O^{-} - B^{(n+1)+} \Rightarrow B^{(n+1)+} - O^{2-} - B^{n+}$$

Owing to this, gastight MICEMs possess an infinite permselectivity.[17] It must be mentioned that the most significant cost associated with partial oxidation of methane (POM) is that of an oxygen plant.[14] Oxygen fluxes obtainable from separation of air using such membranes were found to be commercially feasible for generating synthesis gas by POM. In this industrial application, the following mechanism for POM in a dense ceramic membrane reactor was proposed by Gu et al.[18]

$$CH_4 + 4O_0^{\times} + 8h^{\bullet} \rightarrow CO_2 + 2H_2O + 4\,V_0^{\bullet\bullet}$$

$$CO + O_0^{\times} + 2h^{\bullet} \rightarrow CO_2 + V_0^{\bullet\bullet}$$

$$H_2 + O_0^{\times} + 2h^{\bullet} \rightarrow H_2O + V_0^{\bullet\bullet}$$

$$2O_0^{\times} + 4h^{\bullet} \rightarrow O_2 + 2V_0^{\bullet\bullet}$$

where $O_0^{\times}$, $h^{\bullet}$, and $V_0^{\bullet\bullet}$ stand for lattice oxygen, oxygen vacancy, and electron hole, respectively.

MIECM reactors not only can directly use air as an oxidant, such that products are nitrogen free and environmental pollutants (e.g., NO_x) are not formed during high-temperature reactions, but also can circumvent flammability limits due to diffusion-limited operation. Moreover, the cost of gas compression in downstream processing can be greatly reduced. On the other hand, oxygen separation processes by MIECMs are the most competitive methods for producing pure oxygen at small and intermediate scales in which flexibility of operation is desired, and this method may eventually challenge current commercial applications of cryogenics, pressure-swing adsorptions, and polymeric membranes.[19,20] In addition, MIECM can provide a new way to eliminate atmospheric pollutants by direct thermal decomposition of CO_2 and N_2O.[21]

For practical application of MICEMs in POM to syngas, the membrane materials must be chemically and mechanically stable at high operating temperatures and under harsh environments. Many mixed conductors with the perovskite-type structure have been shown to exhibit notably high oxygen permeability. Unfortunately, most of them are unstable under methane conversion conditions. The $SrCo_{0.8}Fe_{0.2}O_{3.\delta}$ membrane has shown the highest permeability in the (La, Sr) (Co, Fe) O_x series but was found to undergo phase transition under low oxygen pressure or low temperature and decompose under reforming conditions.[1]

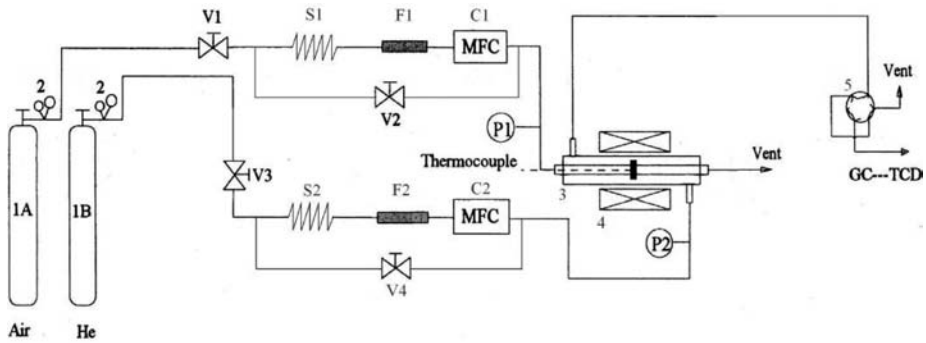

Figure 4. Apparatus used for oxygen permeation measurement. 1A, 1B, gas cylinders; 2, gas regulators; F1−2, filters; S1−2, flow stabilizers; C1−2, mass flow controllers; V1−V4, flow control valves; 3, membrane module; 4, furnace; 5, six-way valves.

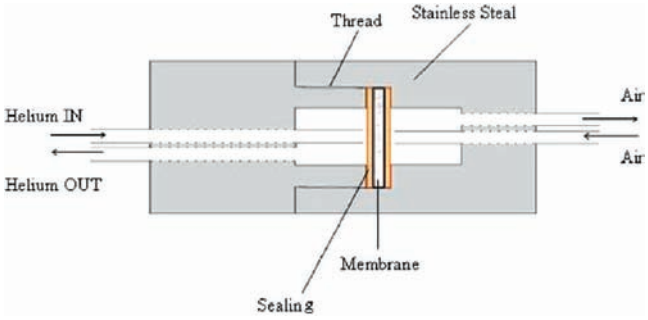

Figure 5. Membrane module.

The performance of the membranes can be affected by many factors such as membrane material, membrane thickness, membrane microstructure, and temperature at which they are to be used. It is well-known that different components can cause different oxygen permeation fluxes. Even with the same component, MIECMs may have quite different oxygen permeation fluxes. The microstructure of a sintered material depends mainly on synthesis methods and conditions used.[22]

Steele stated that oxygen permeation flux higher than 1 $cm^3 \cdot cm^{-2} \cdot min^{-1}$ is always marked for economic interest; however, fluxes around 3.5 $cm^3 \cdot cm^{-2} \cdot min^{-1}$ are usually preferred.[23,24]

Origination of BSCF perovskite and its advantage over related perovskite have been discussed by Zhou et al.[25] In this regard, Teraoka et al. systematically investigated the general trend of oxygen permeation through ceramic membranes based on doped $SrCoO_{3-\delta}$ oxides with the composition of $Ln_{1-x}A_xCo_{1-y}B_yO_{3-\delta}$ (Ln−La, Pr, Nd, Sm, Gd; A = Sr, Ca, Ba; B = Mn, Cr, Fe, Co, Ni, Cu),[26−28] which was closely related to the oxygen ionic and electronic conductivities of the oxides. The highest oxygen permeation flux was found in the $SrCo_{0.8}Fe_{0.2}O_{3-\delta}$ perovskite, in which the La^{3+} ion was totally substituted by the Sr^{2+} ion. Unfortunately, later examination revealed that $SrCo_{0.8}Fe_{0.2}O_{3-\delta}$

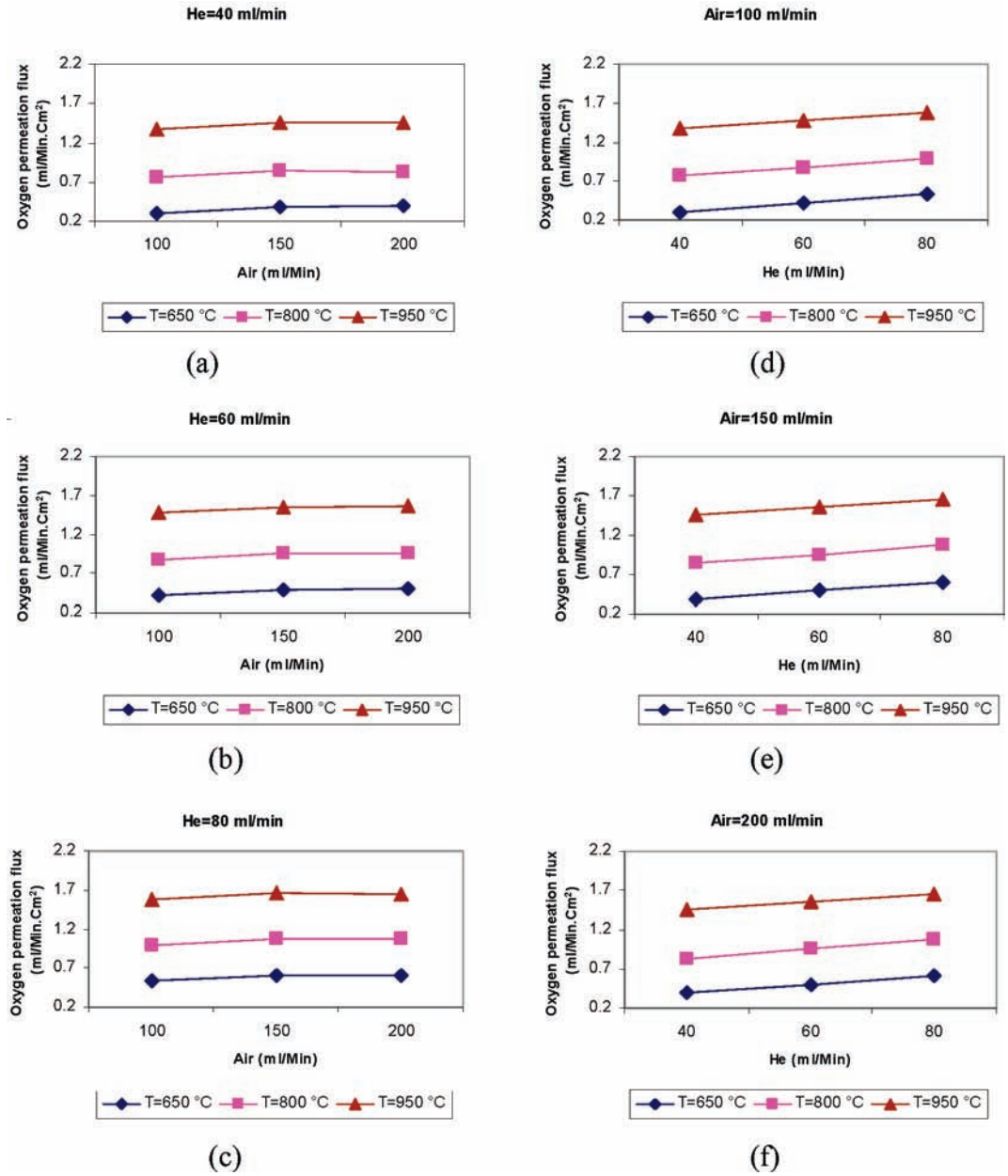

Figure 6. Oxygen permeation flux through the $Ba_{0.2}Sr_{0.8}Co_{0.8}Fe_{0.2}O_{3-\delta}$ disk membrane with a thickness of 4 mm as functions of air flow rate (a, b, and c) in the upstream side and helium flow rate in the downstream side (d, e, and f).

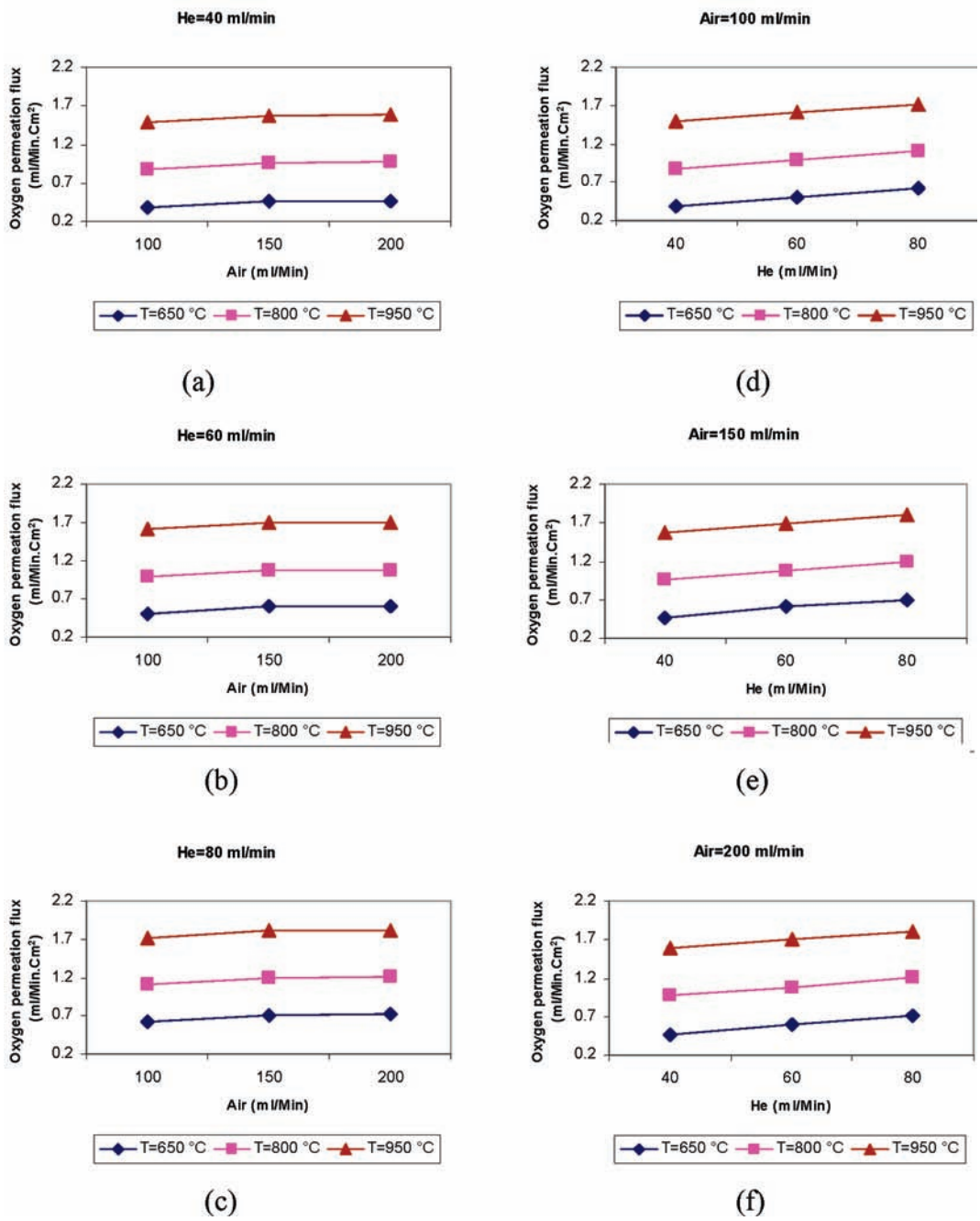

Figure 7. Oxygen permeation flux through the $Ba_{0.5}Sr_{0.5}Co_{0.8}Fe_{0.2}O_{3-\delta}$ disk membrane with a thickness of 4 mm as functions of air flow rate (a, b, and c) in the upstream side and helium flow rate in the downstream side (d, e, and f).

has only limited mechanical and phase stability.[29−31] Although the doping of metal ion(s) with a high valence state on (such as La^{3+}) in the A-site of $SrCo_{0.8}Fe_{0.2}O_{3-\delta}$ could lead to improvement in phase stability of the oxide, the permeability was lowered due to reduction of oxygen vacancy concentration. Partial substitution of iron in the B-site of $SrCo(Fe)O_{3-\delta}$ by other metal ion(s) has also been attempted;[32] the results showed that the best constitution was still cobaltite ferrites doped with alkaline-earth elements.

It was also stated by many researchers that the $SrCo_{0.8}Fe_{0.2}O_{3.\delta}$ membrane shows a high permeation flux of 3.1 $cm^3 \cdot cm^{-2} \cdot min^{-1}$ at 1123 K. Although $SrCo_{0.8}Fe_{0.2}O_{3.\delta}$ exhibits a sufficient oxygen permeation flux for industrial interests, it has weak chemical and structural stability. As a result, there have been attempts to improve the membrane stability. Substitution of Ba with Sr was also claimed to improve the membrane stability. More research has been done to make the $Ba_{0.5}Sr_{0.5}Co_{0.8}Fe_{0.2}O_{0.3-\delta}$ membrane with significant substitution of Ba (50 %).[33−36]

In this research, an attempt to modify the $SrCo_{0.8}Fe_{0.2}O_{3.\delta}$ membrane was undertaken with optimum substitution of Ba with Sr to enhance its chemical and structural stability as well as to keep its high oxygen permeation flux. In other words, this paper focuses on investigation of the oxygen permeation of $Ba_xSr_{1-x}Co_{0.8}Fe_{0.2}O_{0.3-\delta}$ ($x = 0.2$, 0.5, and 0.8) membranes.

As was stated, one of the applications of this study could be applying BSFO membranes for converting methane to synthesis gas. Therefore, two steps were considered for performing the experiments: separation and reaction. Therefore, as a first step,

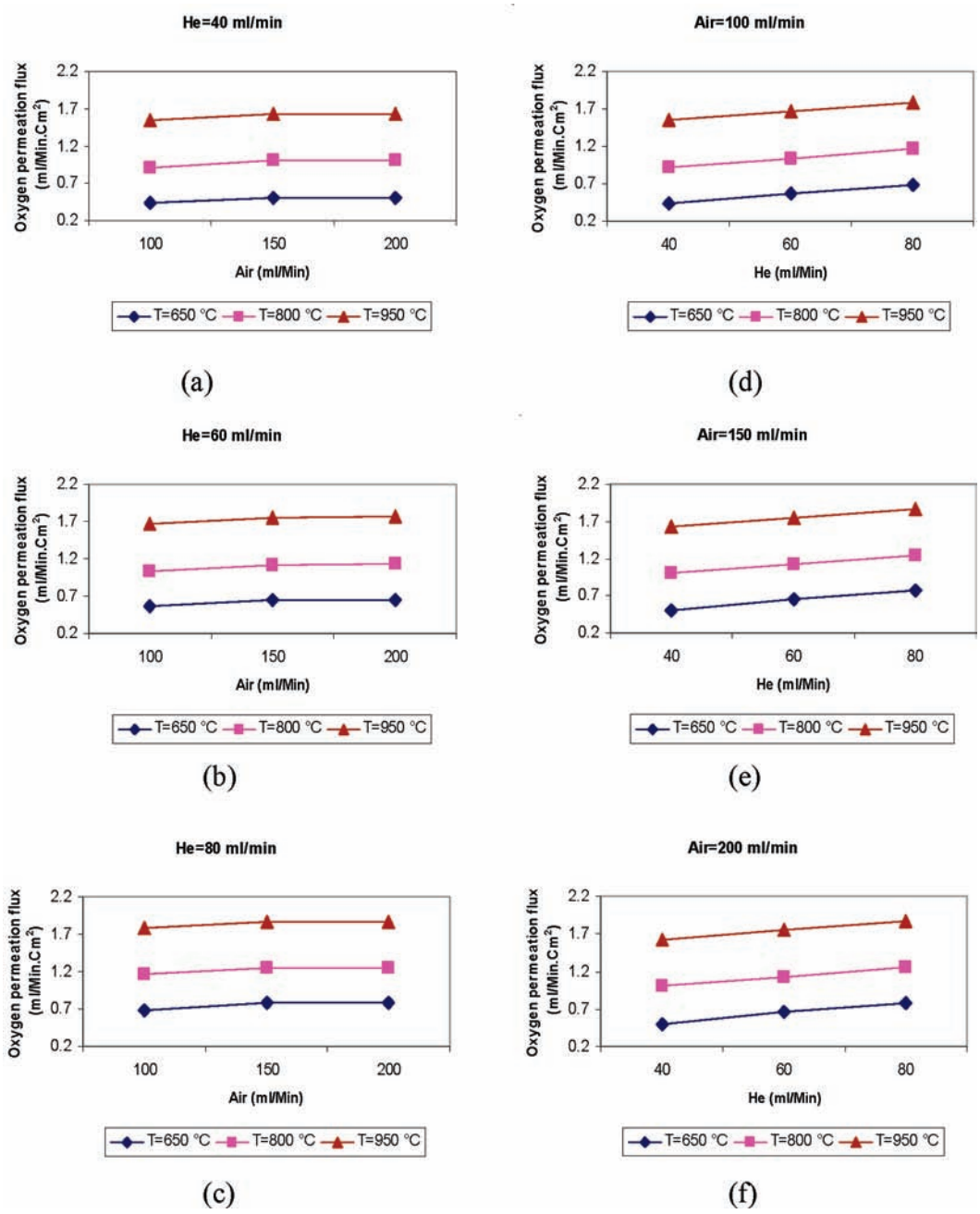

Figure 8. Oxygen permeation flux through the $Ba_{0.8}Sr_{0.2}Co_{0.8}Fe_{0.2}O_{3-\delta}$ disk membrane with a thickness of 4 mm as functions of air flow rate (a, b, and c) in the upstream side and helium flow rate in the downstream side (d, e, and f).

separation performance of the membranes was also considered and studied in this study.

2. Experimental Section

The material powders were synthesized using a combined citrate and EDTA complexing method. $Ba(NO_3)_2$ was first dissolved in EDTA−$NH_3 \cdot H_2O$ solution under heating and stirring. $Sr(NO_3)_2$, $Co(NO_3)_2$, and $Fe(NO_3)_3$ were then added to the solution (All chemicals were purchased from the Merck Company with purities higher than 99.9 %). The mixture was well stirred for about 10 min. Citric acid was then introduced, and the mole ratio of EDTA:citric acid:total metal ions was controlled to be around 1:1.5:1. Precipitation might occur after citric acid addition. $NH_3 \cdot H_2O$ was then added to adjust the pH to 6. EDTA−NH_3 and citrate form a buffering solution, so the pH value of the system is successfully sustained at around 6 during the whole water evaporation process. With evaporation of water, a dark purple gel was obtained. The gel was then pretreated at (120 to 150) °C for several days to make a primary powder, which was calcined at 950 °C for 5 h to obtain a secondary powder with final composition.

According to our previous work,[36] the secondary powder was pressed into disks in a stainless steel mold (21 mm in diameter) under a hydraulic pressure of 2000 bar. These green disks were sintered in a furnace at a temperature of 1100 °C for 10 h with heating and cooling rates of 1 °C·min^{-1}. These conditions were chosen as the best values to cover the common used ranges of the parameters.

As presented in Figures 1(a), 2(a), and 3(a), phase developments of the sintered membranes were studied by X-ray diffraction (XRD), (X-ray Diffraction, Rigaku D-Max/RB with Cu Kα radiation).

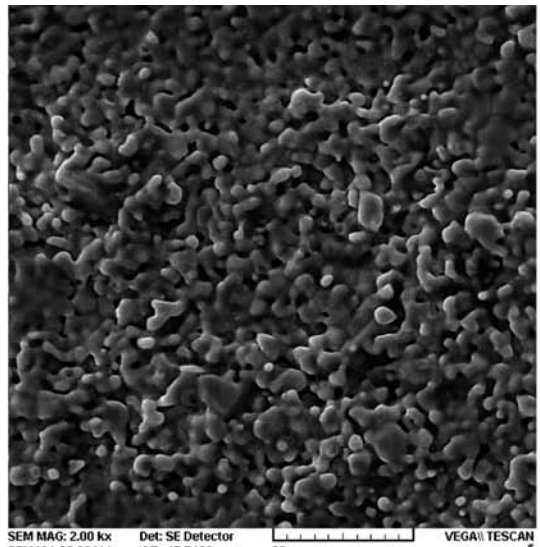

(a)

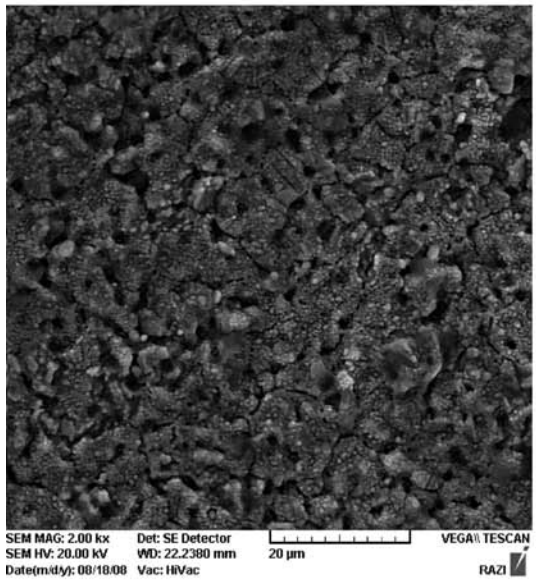

(b)

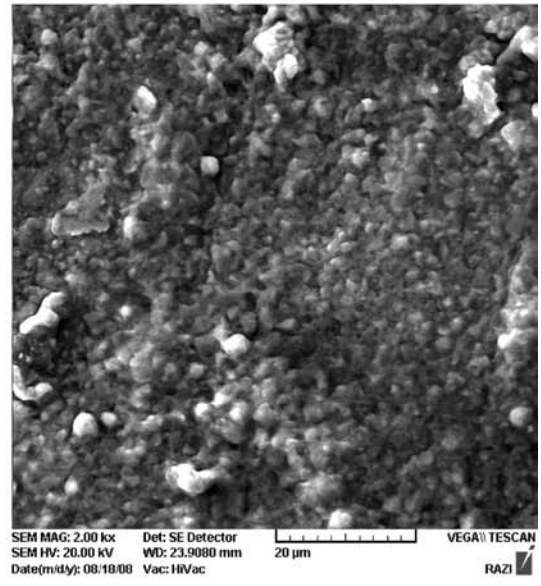

(c)

Figure 9. SEM pictures of the $Ba_{0.2}Sr_{0.8}Co_{0.8}Fe_{0.2}O_{3-\delta}$ disk membrane (a) surface of the fresh membrane; (b) surface of the used membrane exposed to air after 75 h oxygen permeation; (c) surface of the used membrane exposed to helium after 75 h oxygen permeation.

The densities of the sintered membranes were determined by the Archimedes method using distilled water. These densities exceeded 90 % of the theoretical in all cases. The oxygen permeation rates through the membranes were measured using the permeation apparatus as shown in Figure 4. In this work, a simple temperature resistant stainless steel (4841) shell-and-tube permeation module was used as a permeator for the oxygen permeation study. As shown in Figure 5, the disk membrane between two stainless tubes was sealed with ceramic fibers reinforced with high-temperature cement glue (heat resistant to 1200 °C).

Sintered membrane disks were polished to a thickness of 4 mm. The membrane module was surrounded by a tubular furnace, and the operating temperature was measured by a thermocouple. A microprocessor temperature controller (Model BATEC PC 21, Amjad Company, Iran) was used to control the temperature to within ± 1 °C of the set points. Flow rates of the inlet gases were controlled by mass flow controllers (models 8085 Brooks, Company). Air was introduced into the upstream side of the membrane. Helium, as a sweeping gas for the permeating oxygen, was fed to the downstream side of the membrane. Both the upstream and downstream sides were maintained at atmospheric pressure. The effluent streams were analyzed by gas chromatography (Teif Gostar Company, Iran) which was equipped with 2 m 5 Å molecular sieves operated at 24 °C with helium as the carrier gas.

The amount of leakage through pores or cracks due to sealing problems was almost constant in the entire temperature range studied. The leaked oxygen was usually less than 0.1 % of the total oxygen, and in most cases, no nitrogen leakage was detected. It is reasonable to assume that the leaking of nitrogen and oxygen through the pores or cracks is in accordance with the Knudsen diffusion mechanism, so the fluxes of leaked N_2 and O_2 ($J_{N_2}^{Leak}$ and $J_{O_2}^{Leak}$, respectively) can be expressed by the following equation

$$J_{N_2}^{Leak}: J_{O_2}^{Leak} = \sqrt{\left(\frac{32}{38}\right)} \cdot 0.79{:}0.21 \quad (1)$$

The permeation fluxes were then calculated using eq 2

$$J_{O_2}\,(mL \cdot min^{-1} \cdot cm^2) = [C_{O_2} - C_{N_2} \cdot 0.21/0.79 \cdot (28/32)^{1/2}] \cdot \frac{F}{S} \quad (2)$$

where C_{O_2} and C_{N_2} are the measured concentrations of oxygen and nitrogen in the permeation side, respectively; F is flow rate of the sweep gas measured with a soap film flow meter; and S is the membrane area. The flow rate of outlet gas instead of inlet gas (helium) was used for the permeation calculation. In this way, the possible error introduced when using the flow rate of inlet gas, due to the possible leakage of helium from the inner tube to the outer tube, was avoided.[37]

Morphologies of the fresh and used sintered membranes were examined by scanning electron microscopy (VEGAII TESCAN). Crystal structures of the used sintered membranes were characterized with X-ray diffraction (XRD).

3. Results and Discussion

The oxygen permeation properties of BSCFO disk membranes with a thickness of 4 mm were studied at different temperatures, air flow rates, and helium flow rates. Figures 6 to 8 show the influences of air flow rates in the upstream side and helium flow rates in the downstream side on oxygen permeation flux through the prepared membranes at different temperatures of (650, 800, and 950) °C.

As expected, the results show that increasing temperature has a considerable increasing effect on oxygen permeation through the BSCFO disk membranes so that the most permeation appears at the higher temperature of 950 °C. It can be attributed to more oxygen diffusion at higher temperatures. In this regard, increasing temperature leads to a higher oxygen vacancy concentration

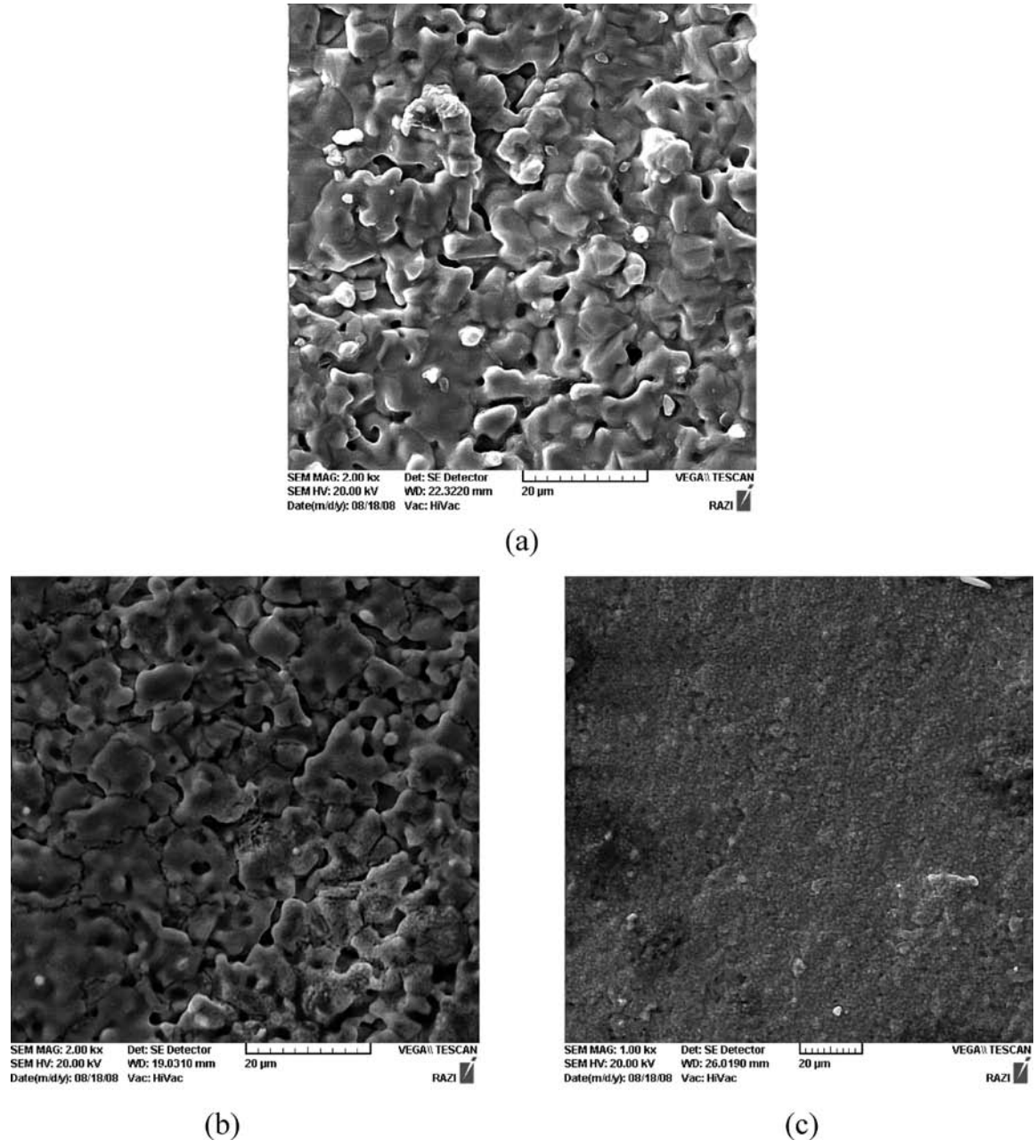

Figure 10. SEM pictures of the $Ba_{0.0.5}Sr_{0.5}Co_{0.8}Fe_{0.2}O_{3-\delta}$ disk membrane (a) surface of the fresh membrane; (b) surface of the used membrane exposed to air after 75 h oxygen permeation; and (c) surface of the used membrane exposed to helium after 75 h oxygen permeation.

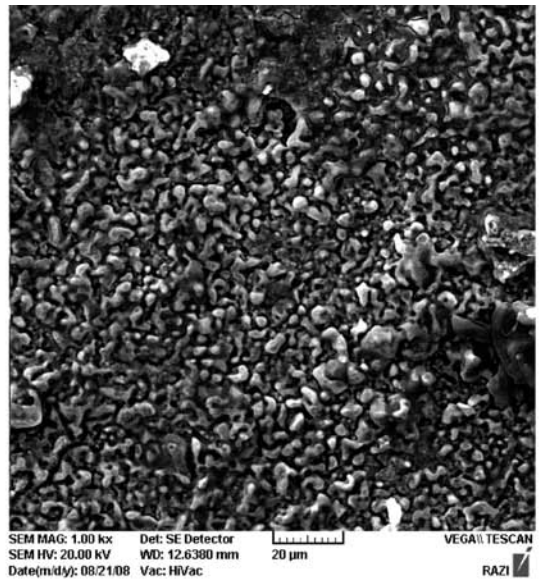

(a)

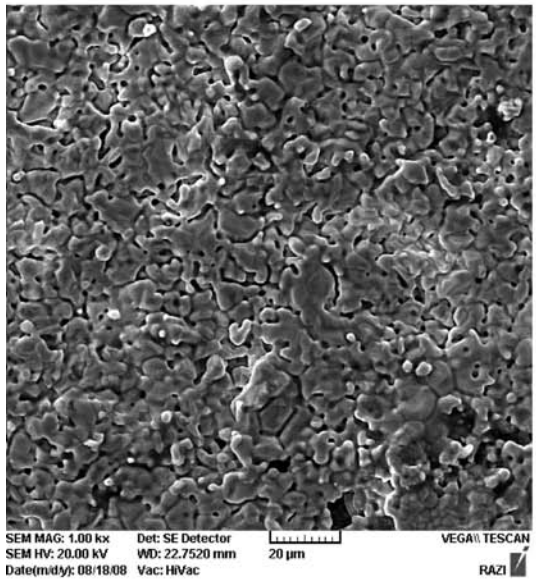

(b)

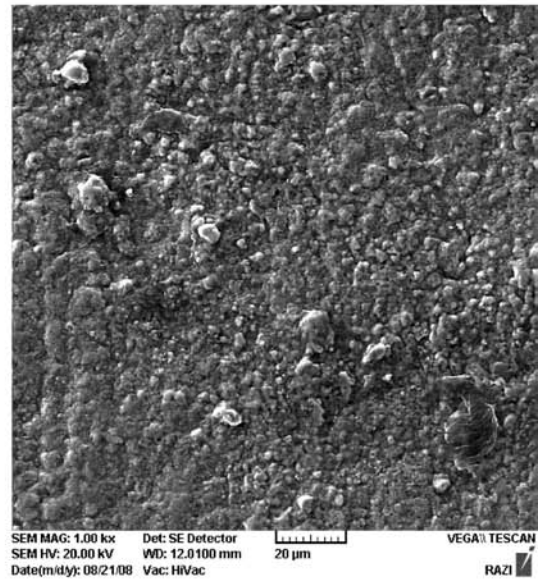

(c)

Figure 11. SEM pictures of the $Ba_{0.08}Sr_{0.2}Co_{0.8}Fe_{0.2}O_{3-\delta}$ disk membrane (a) surface of the fresh membrane; (b) surface of the used membrane exposed to air after 75 h oxygen permeation; and (c) surface of the used membrane exposed to helium after 75 h oxygen permeation.

in perovskite membranes and is responsible for oxygen permeation through the membrane. Also, temperature has a favorable influence on oxygen permeation due to reduction of bulk diffusion and surface reaction resistances. Reduction of the resistances is caused by an increasing diffusion coefficient and surface reaction rates at elevated temperatures.[38]

As shown in Figures 6 to 8 (a to c), the oxygen permeation flux also increases with increasing air flow rate; however, at air flow rates higher than 150 $mL \cdot min^{-1}$, the slope of the trend reduces. It can be interpreted that the exchange rate of oxygen on the membrane surface in the upstream side is not the rate-limiting step for oxygen permeation when the air flow rate is in the range of (150 to 200) $mL \cdot min^{-1}$.

As shown in Figures 6 to 8 (d to f), when the helium flow rate increases from (40 to 80) $mL \cdot min^{-1}$, the oxygen permeation flux also increases. The effect of helium flow rate on the oxygen permeation flux is more significant than that of the air flow rate, as observed. As revealed in Figures 6 to 8, the effects of the mentioned parameters on BSCFO membranes are the same, and increasing the amount of Ba content increases the oxygen permeation flux, so that the oxygen permeation fluxes of $Ba_xSr_{1-x}Co_{0.8}Fe_{0.2}O_{0.3-\delta}$ ($x = 0.2$, 0.5, and 0.8) at the temperature of 950 °C, the air flow rate of 150 $mL \cdot min^{-1}$, and the helium flow rate of 80 $mL \cdot min^{-1}$ are (1.65, 1.80, and 1.86) $mL \cdot min^{-1} \cdot cm^{-2}$ for the membranes with a thickness of 4 mm, respectively.

It must be mentioned that these results were obtained when the oxygen partial pressure in the upstream side was 0.21 and total pressure was atmospheric. It can be expected that with increasing pressure in the upstream side and reduction of the membrane thickness the higher amount of oxygen permeation flux can be obtained, and the results can meet the value suggested by Bredesen and Sogge for competition with other traditional processes.[39]

Table 1. EDS Results of the Fresh $Ba_{0.2}Sr_{0.8}Co_{0.8}Fe_{0.2}O_{3-\delta}$ Disk Membrane and the Used $Ba_{0.2}Sr_{0.8}Co_{0.8}Fe_{0.2}O_{3-\delta}$ Disk Membrane after 75 h Oxygen Permeation

	atomic (%)				
	O	Fe	Co	Sr	Ba
fresh disk membrane	12.51	9.17	35.21	37.87	5.24
surface exposed to air of the used disk membrane	12.24	8.81	36.23	35.19	7.52
surface exposed to helium of the used disk membrane	52.19	1.44	6.46	32.53	6.63

Table 2. EDS Results of the Fresh $Ba_{0.5}Sr_{0.5}Co_{0.8}Fe_{0.2}O_{3-\delta}$ Disk Membrane and the Used $Ba_{0.5}Sr_{0.5}Co_{0.8}Fe_{0.2}O_{3-\delta}$ Disk Membrane after 75 h Oxygen Permeation

	atomic (%)				
	O	Fe	Co	Sr	Ba
fresh disk membrane	36.84	5.18	20.26	17.14	20.57
surface exposed to air of the used disk membrane	20.93	8.38	31.57	21.84	17.32
surface exposed to helium of the used disk membrane	37.27	4.25	24.16	21.24	13.08

Table 3. EDS Results of the Fresh $Ba_{0.8}Sr_{0.2}Co_{0.8}Fe_{0.2}O_{3-\delta}$ Disk Membrane and the Used $Ba_{0.8}Sr_{0.2}Co_{0.8}Fe_{0.2}O_{3-\delta}$ Disk Membrane after 75 h Oxygen Permeation

	atomic (%)				
	O	Fe	Co	Sr	Ba
fresh disk membrane	8.52	8.41	33.09	7.02	42.96
surface exposed to air of the used disk membrane	6.59	6.86	27.28	13.48	45.79
surface exposed to helium of the used disk membrane	10.65	8.18	32.61	16.80	31.76

The fresh and used membranes were analyzed with SEM and EDS. SEM pictures of the disk BSCFO membranes are shown in Figures 9 to 11. For the fresh membranes as shown in Figures 9(a) to 11(a), ceramic grains with their boundaries are visible. For the used $Ba_{02}Sr_{0.8}Co_{0.8}Fe_{0.2}O_{3-\delta}$ membrane after 75 h oxygen permeation as shown in Figure 9(b), the surface exposed to air (feed side) is blurry, and it seems that some material is deposited on the membrane surface; however, the EDS analysis shows that there is no other deposited material. As shown in Figures 9(b) to 11(b), the surfaces of membranes exposed to air (feed side) tend to fusion among grains.

As observed in Figure 9(c) to 11(c), the surfaces of membranes exposed to helium (permeate side) strongly tend to coalesce, so that the surfaces of $Ba_{(x=0.5\text{ and }0.8)}Sr_{1-x}Co_{0.8}Fe_{0.2}O_{3-\delta}$ membranes have steady flat surfaces totally different from those of the fresh membranes.

The element compositions of the fresh membranes and the used membranes are presented in Tables 1 to 3. The results show that the surfaces of membranes exposed to helium are totally different from the fresh membrane surfaces and the membrane surfaces exposed to air.

Figures 1(a) to 3(a) show XRD patterns of the fresh BSCFO membranes. Figures 1(b and c) to 3(b and c) are XRD patterns of the used membrane surfaces exposed to air and the used membrane surfaces exposed to helium for 75 h oxygen permeation at 950 °C, respectively. The used disk membranes were cooled from the oxygen permeation condition to room temperature with a rate of 1 °C·min^{-1}. Figures 1 to 3 reveal that the fresh membrane is cubic perovskite, and the surfaces of the BSCFO disk membranes exposed to air after the 75 h oxygen permeation test still keep their perovskite structure. Also, the surface of the $Ba_{0.2}Sr_{0.8}Co_{0.8}Fe_{0.2}O_{3-\delta}$ disk membrane exposed to helium after the 75 h oxygen permeation test still keeps its perovskite structure. However, no perovskite structure is observed on the $Ba_{(x=0.5\text{ and }0.8)}Sr_{1-x}Co_{0.8}Fe_{0.2}O_{3-\delta}$ membrane surfaces exposed to helium. So, it can be concluded that the $Ba_{0.2}Sr_{0.8}Co_{0.8}Fe_{0.2}O_{3-\delta}$ disk membrane is more stable than the others. A reduction of peak intensities shows that the crystalline structure changes to some extent. Figures 1(b and c) show that there is a small amount of Sr and hematite and cobalt oxide in crystalline form on the membrane surfaces exposed to air and helium, respectively. Also, Figures 2 and 3(b and c) reveal that there are amounts of Fe, Co, and iron(II) sulfide and cobalt oxide in crystalline form on the membrane surfaces exposed to helium. Formation of the metal sulfide can be attributed to the interaction of trace amounts (< 1000 ppm according to the gas purities) of SO_2 in air and helium with the surfaces of the membranes.

4. Conclusion

The BSCFO disk membranes were prepared by isostatic pressing. The oxygen permeation flux of the BSCFO membranes with a thickness of 4 mm as functions of air flow rate in the upstream side and helium flow rate in the downstream side at temperatures of (650, 800, and 950) °C was investigated. It was found out that the oxygen permeation flux increases significantly with temperature. Also, it increases with increasing helium flow rate in the downstream side.

However, the oxygen permeation flux increases with increasing air flow rate in the upstream side, when it is less than 150 mL·min^{-1}. This effect is less significant at higher air flow rates. As a result, it can be said that the effect of increasing helium flow rate downstream is much more significant than that of increasing air flow rate.

EDS and XRD analysis showed that although characteristics of the used disk membrane surface exposed to air are similar to the fresh disk membrane surface characteristics of the used disk membrane surface exposed to helium are different.

It was also found out that the effects of all mentioned parameters on BSCFO membranes are the same, and increasing the amount of Ba content increases the oxygen permeation flux.

The largest oxygen permeation fluxes achieved in this study were (1.65, 1.80, and 1.86) mL·min^{-1}·cm^{-2} for the BSCFO membranes with a thickness of 4 mm, at a temperature of 950 °C, an air flow rate of 150 mL·min^{-1}, and a helium flow rate of 80 mL·min^{-1}, respectively. The novel achievement of the present research compared with the other research[22,24] is that the synthesized $Ba_xSr_{1-x}Co_{0.8}Fe_{0.2}O_{0.3-\delta}$ ($x = 0.2$, 0.5, and 0.8) membranes have an admirable amount of oxygen permeation fluxes for economic industrial interests, and due to the high mechanical stability of $Ba_{0.2}Sr_{0.8}Co_{0.8}Fe_{0.2}O_{3-\delta}$, it can hopefully be further improved by reduction of its thickness.

Literature Cited

(1) Dong, H.; Shao, Z.; Xiong, G.; Tong, J. S.; Yang, W. Investigation on POM reaction in a new perovskite membrane reactor. *Catal. Today* **2001**, *67*, 3–13.

(2) Wilhelm, D. J.; Simbeck, D. R.; Karp, A. D.; Dickenson, R. L. Syngas production for gas-to-liquids applications: technologies, issues and outlook. *Fuel Process. Technol.* **2001**, *71*, 139–148.

(3) Woo, S. K.; Lee, S.; Lee, K. S. Surface Reactive Coatings on Oxygen Permeable Ceramic Membranes. *The Fifth International Membrane Science & Technology Conference*; The University of New South Wales: Sydney, Australia, 2003.

(4) Saracco, G.; Versteeg, G. F.; Van Swaaij, W. P. M. Current hurdles to the success of high-temperature membrane reactors. *J. Membr. Sci.* **1994**, *95*, 105–123.

(5) Bouwmeester, H. J. M.; Burggraaf, A. J. Dense ceramic membranes for oxygen separation. *Fundamentals of Inorganic Membrane Science and Technology*; Burggraaf, A. J., Cot, L., Eds.; Elsevier: Amsterdam, 1996' pp 435−528.

(6) Balachandran, U.; Dusek, J. T.; Mieville, R. L.; Poeppel, R. B.; Kleefisch, M. S.; Pei, S.; Kobylinski, T. P.; Udovich, C. A.; Bos, A. C.

Dense ceramic membranes for partial oxidation of methane to syngas. *Appl. Catal. A: Gen.* **1995**, *133*, 19–29.
(7) Ten Elshof, J. E.; Bouwmeester, H. J. M.; Verweij, H. Oxidative coupling of methane in a mixed-conducting perovskite membrane reactor. *Appl. Catal. A: Gen.* **1995**, *130*, 195–212.
(8) Lin, Y. S.; Zeng, Y. Catalytic properties of oxygen semipermeable perovskite-type ceramic membrane materials for oxidative coupling of methane. *J. Catal.* **1996**, *164*, 220–231.
(9) Dong, H.; Shao, Z. P.; Liu, S. L.; Xiong, G. X.; Yang, W. S. Partial oxidation of methane to syngas in a mixed-conducting membrane reactor. *Chin. Sci. Bull.* **1999**, *44*, 2050–2052.
(10) Kharton, V. V.; Naumovich, E. N.; Nikolaev, A. V. Materials of high-temperature electrochemical oxygen membranes. *J. Membr. Sci.* **1996**, *111*, 149–157.
(11) Qiu, L.; Lee, T. H.; Yang, L. Y. L.; Jacobson, A. J.; Liu, L. M. Oxygen permeation studies of $SrCO_{0.8}Fe_{0.2}O_3$. *Solid State Ionics* **1995**, *76*, 321–329.
(12) Roy, R. Multiple ion substitution in the perovskite lattice. *J. Am. Ceram. Soc.* **1954**, *37*, 581–588.
(13) Bhalla, A. S.; Guo, R.; Roy, R. The perovskite structure - a review of its role in ceramic science and technology. *Mater. Res. Innovat.* **2000**, *4*, 3–26.
(14) Kharton, V.; Yaremchenko, A.; Kovalevsky, V.; Viskup, A. P.; Naumovich, E. N.; Kerko, P. F. Perovskite-type oxides for high-temperature oxygen separation membranes. *J. Membr. Sci.* **1999**, *163*, 307–317.
(15) Liu, Y.; Tan, X.; Li, K. Mixed Conducting Ceramics for Catalytic Membrane Processing. *Catal. Rev.* **2006**, *48*, 145–198.
(16) Shao, Z.; Xiong, G.; Tong, J.; Dong, H.; Yang, W. Ba effect in doped $Sr(Co_{0.8}Fe_{0.2})O_{3-\delta}$ on the phase structure and oxygen permeation properties of the dense ceramic membranes. *Sep. Purif. Technol.* **2001**, *25*, 419–429.
(17) Shao, Z.; Xiong, G.; Cong, Y.; Yang, W. Synthesis and oxygen permeation study of novel perovskite-type $BaBi_xCo_{0.2}Fe_{0.8-x}O_{3-\delta}$ ceramic membranes. *J. Membr. Sci.* **2000**, *164*, 167–176.
(18) Gu, X.; Jin, W.; Chen, C.; Xu, N.; Shi, J.; Ma, Y. H. YSZ-$SrCo_{0.4}Fe_{0.6}O_{3-\delta}$ Membranes for the Partial Oxidation of Methane to Syngas. *AIChE J.* **2002**, *48*, 2051–2060.
(19) Itoh, N.; Sanchez, C. M. A.; Xu, W. C.; Haraya, K.; Hongo, M. Application of a membrane reactor system to thermal decomposition of CO_2. *J. Membr. Sci.* **1993**, *77*, 245–253.
(20) Teraoka, Y.; Matsumura, Y.; Asakura, K.; Kagawa, S. Application of mixed conductive La-Sr-Co-Fe perovskites to NO_x removal membrane reactors. *Solid State Ionics* **1999**, *99*, 131–138.
(21) Tong, J.; Yang, W.; Zhu, B.; Cai, R. Investigation of ideal zirconium-doped Perovskite-type ceramic membrane materials for oxygen separation. *J. Membr. Sci.* **2002**, *203*, 175–189.
(22) Ten Elshof, J. E.; Bouwmeester, H. J. M.; Verweij, H. Oxygen transport through $La_{1-x}Sr_xFeO_{3-\delta}$ membranes. I. *Solid State Ionics* **1995**, *81*, 97–109.
(23) Steele, B. C. H. Oxygen ion conductors and their technological application. *Mater. Sci. Eng.* **1992**, *B13*, 79–87.
(24) Steele, B. C. H. Ceramic ion conducting membranes. *Curr. Opin. Solid State Mater. Sci.* **1996**, *1*, 684–691.
(25) Zhou, W.; Ran, R.; Shao, Z. Progress in understanding and development of $Ba_{0.5}Sr_{0.5}Co_{0.8}Fe_{0.2}O_{3-\delta}$-based cathodes for intermediate-temperature solid-oxide fuel cells: A review. *J. Power Sources* **2009**, *192*, 231–246.
(26) Teraoka, Y.; Zhang, H. M.; Furukawa, S.; Yamazoe, N. Oxygen permeation through perovskite-type oxides. *Chem. Lett.* **1985**, *14*, 1743–1746.
(27) Teraoka, Y.; Nobunaga, T.; Yamazoe, N. Effect of cation substitution on the oxygen semipermeability of perovskite oxide. *Chem. Lett.* **1988**, *17*, 503–506.
(28) Teraoka, Y.; Nobunaga, T.; Okamoto, K.; Miura, N.; Yamazoe, N. Influence of constituent metal cations in substituted LaCoO3 on mixed conductivity and oxygen permeability. *Solid State Ionics* **1991**, *48*, 207–212.
(29) Qiu, L.; Lee, T. H.; Liu, L. M.; Yang, Y. L.; Jacobson, A. J. Oxygen permeation studies of $SrCo_{0.8}Fe_{0.2}O_{3-\delta}$. *Solid State Ionics* **1995**, *76*, 321–329.
(30) Pei, S.; Kleefisch, M. S.; Kobylinski, T. P.; Faber, J.; Udovich, C. A.; Zhang-McCoy, V.; Dabrowski, B.; Balachandran, U.; Mieville, R. L.; Poeppel, R. B. Failure mechanisms of ceramic membrane reactors in partial oxidation of methane to synthesis gas. *Catal. Lett.* **1995**, *30*, 201–212.
(31) Kruidhof, H.; Bouwmeester, H. J. M.; V. Doorn, R. H. E.; Burggraaf, A. J. Influence of Order-Disorder Transitions on Oxygen Permeability through Selected Nonstoichiometric Perovskite-Type Oxides. *Solid State Ionics* **1993**, *63−65*, 816–822.
(32) Kharton, V. V.; Tikhonovich, V. N.; Li, S. B.; Naumovich, E. N.; Kovalevsky, A. V.; Viskup, A. P.; Bashmakav, I. A.; Yaremchenko, A. A. Ceramic microstructure and oxygen permeability of SrCo(Fe, M)$O_{3-\delta}$ (M = Cu or Cr) perovskite membranes. *J. Electrochem. Soc.* **1998**, *145*, 1363–1373.
(33) Qiu, L.; Lee, T. H.; Liu, L. M.; Yang, Y. L.; Jacobson, A. J. Oxygen permeation studies of $SrCo_{0.8}Fe_{0.2}O_{3-\delta}$. *Solid State Ionics* **1995**, *76*, 321–329.
(34) Pei, S.; Kleefisch, M. S.; Kobylinski, T. P.; Faber, J.; Udovich, C. A.; Zhang-McCoy, V.; Dabrowski, B.; Balachandran, U.; Mieville, R. L.; Poeppel, R. B. Failure mechanisms of ceramic membrane reactors in partial oxidation of methane to synthesis gas. *Catal. Lett.* **1995**, *30*, 201–212.
(35) Wang, H.; Cong, Y.; Yang, W. Oxygen permeation study in a tubular $Ba_{0.5}Sr_{0.5}Co_{0.8}Fe_{0.2}O_{3-\delta}$ oxygen permeable membrane. *J. Membr. Sci.* **2002**, *210*, 259–271.
(36) Mosadeghkhah, A.; Alaee, M. A.; Mohammadi, T. Effect of sintering temperature and dwell time and pressing pressure on $Ba_{0.5}Sr_{0.5}Co_{0.8}Fe_{0.2}O_{3-\delta}$ perovskite-type membranes. *Mater. Des.* **2007**, *28*, 1699–1706.
(37) Shao, Z. P.; Yang, W. S.; Cong, Y.; Dong, H.; Tong, J. H.; Xiong, G. X. Investigation of the permeation behavior and stability of a $Ba_{0.5}Sr_{0.5}Co_{0.8}Fe_{0.2}O_{3-\delta}$ oxygen membrane. *J. Membr. Sci.* **2000**, *172*, 177–188.
(38) Yang, Z.; Lin, Y. S. A semi-empirical equation for oxygen nonstoichiometry of perovskite-type ceramics. *Solid State Ionics* **2002**, *150*, 245–254.
(39) Bredesen, R.; Sogge, J. *Paper Presented at The United Nations Economic Commission for Europe Seminar on Ecological Applications of Innovative Membrane Technology in Chemical Industry*, Chem/Sem. 21/R.12, Cetaro, Calabria, Italy, 1−4 May 1996.

Received for review February 14, 2009. Accepted September 3, 2009. The authors gratefully acknowledge financial support from the Petrochemical Research and Technology Company (Grant No. 83111190).

JE9001762